

---

# Spectrum concentration in deep residual learning: a free probability approach

---

**Zenan Ling**

Department of Electrical Engineering  
Shanghai Jiaotong University  
Shanghai 200240, China  
lingzenan@sjtu.edu.cn

**Robert C. Qiu**

Department of Electrical and Computer Engineering  
Tennessee Technological University  
Cookeville, TN 38505, USA  
rqiu@tntech.edu

## Abstract

We revisit the initialization of deep residual networks (ResNets) by introducing a novel analytical tool in free probability to the community of deep learning. This tool deals with *non-Hermitian* random matrices, rather than their conventional *Hermitian* counterparts in the literature. As a consequence, this new tool enables us to evaluate the singular value spectrum of the input-output Jacobian of a fully-connected deep ResNet for both linear and nonlinear cases. With the powerful tool of free probability, we conduct an asymptotic analysis of the spectrum on the single-layer case, and then extend this analysis to the multi-layer case of an arbitrary number of layers. In particular, we propose to rescale the classical random initialization by the number of residual units, so that the spectrum has the order of  $O(1)$ , when compared with the large width and depth of the network. We empirically demonstrate that the proposed initialization scheme learns at a speed of orders of magnitudes faster than the classical ones, and thus attests a strong practical relevance of this investigation.

## 1 Introduction

Deep neural networks have obtained impressive achievements in numerous fields from computer vision [12] to speech recognition [13] and natural language processing [3]. Yet for all the successes won with these deep structures, we have gained only a rudimentary understanding of why and in what contexts they work well. It has been well-known that the weight initialization plays a key role in the training of deep models. Prior works [5, 7, 15] have shown that, to prevent gradients from vanishing or exploding, one shall choose a proper initialization so that the deep network's input-out Jacobian is well-conditioned. In other words, in order to preserve the norm of a randomly chosen error vector through backpropagation, the mean squared singular value of the Jacobian matrix remains to be the order of  $O(1)$ , compared with the (possibly) tremendous width or depth of the network. We refer to this property as the "Spectrum Concentration" of the Jacobian matrix, that is different from the similar concept of "Dynamical Isometry" [17] demanding that *all* singular values remain close to 1.

In particular, ResNet, as a super star among these deep structures, has achieved the state-of-the-art performance on various challenging tasks [8, 9]. For example, the He initialization [7] and the batch normalization (BN) technique [10] are commonly combined together to ensure an effective training of ResNets. Experiments in Figure 1 show, however, that the input-output Jacobian of a fully-connected ResNet (without BN) with He's initialization can be ill-conditioned, in that most singular values are close to zero, and there is a tail consisting of extremely large singular values. This occurs even at the *beginning* of the training procedure. Recall that, before the introduction of BN, various of deep networks have been successfully designed and trained without this catastrophic

problem of exploding or vanishing gradients. This surprising empirical result naturally leads to the following question: *Have we really used the “good” initialization for ResNets?*

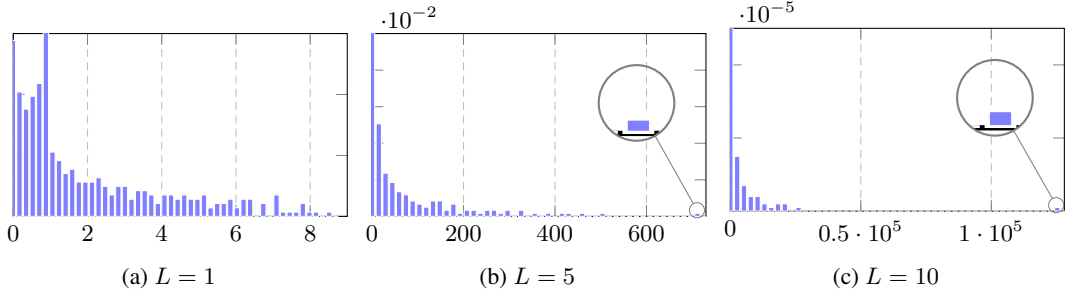


Figure 1: Empirical eigenvalue density of  $\mathbf{J}\mathbf{J}^T$  with  $\mathbf{J}$  the input-output Jacobian of a fully connected (untrained) ResNet of width  $N = 400$  and depth  $L = 1, 5, 10$  with  $\sigma_w^2 = 2$ .

Among the commonly used random initialization schemes, the variances of the Gaussian weights are *always* normalized by the numbers of neurons of the corresponding layer (i.e., the *width* of the network). In contrast, the number of layers of the network (i.e., its *depth*), as another crucial parameter, has been rarely taken into account in the models. In this article, exploiting advanced tools in random matrix theory in the regime of large network width and depth, we prove that, for ResNets, the variance of the random weights should *also* be scaled as a function of the number of layers.

### 1.1 Related work

The authors in [17] argue that random Gaussian initialization results in an ill-conditioned Jacobian, and propose to use orthogonal weights initialization to achieve dynamical isometry in deep *linear* networks. The recent works [15, 16] open the door for a direct application of random matrix theory, particularly *free probability*, to evaluating the Jacobian spectrum of a deep network, in which the singular value distribution of the Jacobian of a fully-connected network is analytically given as a function of depth, random initialization and nonlinearity. In [6] the authors prove the existence of a global optimal solution for linear ResNets, if the spectral norms of the weights are bounded by  $O(1/L)$  and therefore, small random weights that is normalized by the layer number  $L$ , helps deep residual learning.

### 1.2 Our contributions

We extend the framework established in [15] to a non-Hermitian setting in order to overcome the (non-trivial) technical difficulty (mentioned in 3.1) arising from studying the spectrum of the input-output Jacobian of a single layer ResNet. This result is then extended to the multi-layer case, for which we calculate the expectation and variance of the *full* spectrum to ensure the “Spectrum Concentration”. It suffices to take  $\sigma_w^2 = O(L^{-1})$  to ensure the mean squared singular value of the aforementioned Jacobian to be of order  $O(1)$ . Besides, the full spectrum characterization in linear case is provided. The theoretical results are corroborated by empirical evidences on popular CIFAR-10 dataset. Detailed proofs and complementary experiments are deferred to supplementary materials (SM) due to space limitation.

## 2 Problem Statement and Preliminaries

### 2.1 Problem set up

Denote the output vector of the  $(l - 1)$ -th layer  $\mathbf{x}^l \in \mathbb{R}^N$ , weight matrix  $\mathbf{W}^l \in \mathbb{R}^{N \times N}$  and bias vectors  $\mathbf{b}^l \in \mathbb{R}^N$  of the layer  $l$ , then a residual unit of a fully connected ResNet<sup>1</sup> without BN of depth  $L$  is given by:

$$\mathbf{x}^l = \mathbf{x}^{l-1} + \mathbf{W}^l \phi(\mathbf{x}^{l-1}) + \mathbf{b}^l \quad \text{for } l = 1, \dots, L, \quad (1)$$

<sup>1</sup>We consider the “full pre-activation” ResNet proposed in [9].

where  $\mathbf{x}_0 \in \mathbb{R}^N$  is the input data of the network and  $\phi : \mathbb{R} \mapsto \mathbb{R}$  denotes the pointwise nonlinearity. The associated input-output Jacobian is given by

$$\mathbf{J} = \frac{\partial \mathbf{x}^L}{\partial \mathbf{x}^0} = \prod_{l=1}^L (\mathbf{I}_N + \mathbf{W}^l \mathbf{D}^l). \quad (2)$$

with diagonal  $\mathbf{D}^l$  such that  $\mathbf{D}_{ii}^l = \phi'(\mathbf{x}_i^{l-1})$ .

We are interested in the initial state of the training procedure of a ResNet described in (1) by considering two popular random weight initializations: (1) random Gaussian weights with  $\mathbf{W}_{ij}^l \sim \mathcal{N}(0, \sigma_w^2/N)$ , and (2) random orthogonal weights that satisfies  $\mathbf{W}^l (\mathbf{W}^l)^\top = \sigma_w^2 \mathbf{I}_N$ . Moreover, two nonlinearities: ReLU and hard-tanh, are explored. For both of the nonlinearities, the diagonal entries of  $\mathbf{D}^l$  follows a Bernoulli distribution with parameter  $p_l$ , measuring the probability of neuron excitation of the layer  $l$ .

In order to study the initialization dynamics of the ResNet, our objective is to control the eigenvalue spectrum of  $\mathbf{J}\mathbf{J}^\top$ , which shall be carried out through advanced techniques of random matrix theory and free probability, which we subsequently introduce.

## 2.2 A review of free probability: the Stieltjes, M-, R- and S-transform

Free probability generalizes probability theory to algebras of non-commutative random variables, which is notably the case of the algebra of random matrices [14, 20]. When a pair of random matrices is free, the eigenvalue distribution of their combinations (sum, product, etc.) can then be determined through specific analytical tools, introduced next.<sup>2</sup>

The spectral density of a random Hermitian matrix  $\mathbf{X} \in \mathbb{R}^{N \times N}$  is defined as  $\rho_{\mathbf{X}}(\lambda) = \frac{1}{N} \sum_{k=1}^N \delta(\lambda - \lambda_k(\mathbf{X}))$ , where  $\lambda_k(\mathbf{X})$  ( $k = 1, \dots, N$ ) denote the  $N$  eigenvalues of  $\mathbf{X}$ . The limiting spectral density is defined as the limit of  $\rho_{\mathbf{X}}(\lambda)$  as  $N \rightarrow \infty$ , if it exists.

The Stieltjes transform of  $\rho_{\mathbf{X}}$  is defined as  $G_{\mathbf{X}}(z) = \int_{\mathbb{R}} \frac{\rho_{\mathbf{X}}(t)}{z-t} dt$ , where  $z \in \{z : z \in \mathbb{C}, \Im(z) > 0\}$ . The spectral density can be recovered from the Stieltjes transform using the inversion formula,  $\rho_{\mathbf{X}}(\lambda) = -\frac{1}{\pi} \lim_{\epsilon \rightarrow 0^+} \Im G_{\mathbf{X}}(\lambda + i\epsilon)$ . The Stieltjes transform can be typically expanded into a power series with coefficients as  $G_{\mathbf{X}}(z) = \sum_{k=0}^{\infty} \frac{m_k}{z^k}$ , with the matrix moments  $m_k = \int d\lambda \rho(\lambda) \lambda^k$ , which further determine the moment generating function  $M_{\mathbf{X}}$  (also referred to as the M-transform) of the random matrix  $\mathbf{X}$ ,

$$M_{\mathbf{X}}(z) = zG_{\mathbf{X}}(z) - 1 = \sum_{k=1}^{\infty} \frac{m_k}{z^k}. \quad (3)$$

Moreover, with the Lagrange inversion theorem [4], we have

$$M_{\mathbf{X}}^{-1}(z) = \frac{m_1}{z} + \frac{m_2}{m_1} + \dots, \quad (4)$$

The Stieltjes transform is a very versatile transform to study the random matrices [19], but when dealing with sums and products of free random matrices, the related R- and S-transform, defined as follows, are more convenient:

$$R_{\mathbf{X}}(z) = G_{\mathbf{X}}^{-1}(z) - \frac{1}{z}, \quad S_{\mathbf{X}}(z) = \frac{1+z}{zM_{\mathbf{X}}^{-1}(z)}. \quad (5)$$

For any two freely independent non-commutative random variables  $\mathbf{X}, \mathbf{Y}$ , the R- and S-transform have the following definite (convolution) properties,

$$R_{\mathbf{X}+\mathbf{Y}}(z) = R_{\mathbf{X}}(z) + R_{\mathbf{Y}}(z), \quad S_{\mathbf{X}\mathbf{Y}}(z) = S_{\mathbf{X}}(z)S_{\mathbf{Y}}(z). \quad (6)$$

As such, the R-transform *linearizes* free additive convolution and the S-transform of the matrix multiplication  $\mathbf{X}\mathbf{Y}$  is simply the multiplication of their S-transforms. Both R- and S-transforms relate through [14],

$$S_{\mathbf{X}}(zR_{\mathbf{X}}(z)) = \frac{1}{R_{\mathbf{X}}(z)}. \quad (7)$$

<sup>2</sup> In the section that follows, the argument  $z$  will be frequently dropped for notational simplicity.  $f^{-1}$  denotes the functional inverse of  $f$ .

### 3 Theoretical results

Equipped with the aforementioned free probability tool, we are in a position to study the asymptotic spectrum of the Jacobian matrix in the simultaneously large  $N, L$  limit.

#### 3.1 Single layer case

Let  $\mathbf{J}_l := \mathbf{I} + \mathbf{W}^l \mathbf{D}^l$  denotes the input-output Jacobian matrix of the layer  $l$ . Expand  $\mathbf{J}_l \mathbf{J}_l^\top$  and we have that

$$\mathbf{J}_l \mathbf{J}_l^\top = \mathbf{I} + \mathbf{W}^l \mathbf{D}^l \mathbf{D}^l (\mathbf{W}^l)^\top + \mathbf{W}^l \mathbf{D}^l + \mathbf{D}^l (\mathbf{W}^l)^\top. \quad (8)$$

Note that the objective of interest  $\mathbf{J}_l \mathbf{J}_l^\top$  is Hermitian but the resulting four terms of expansion are not freely independent and thus can not be handled with a single R-transform. On the other hand, the term in  $\mathbf{J}_l$  are *free* but they are *non-Hermitian*. As such, we perform an extension of conventional (Hermitian) free probability to non-Hermitian random matrices to evaluate the limiting eigenvalue distribution of  $\mathbf{J}_l \mathbf{J}_l^\top$ . Consider a Hermitian matrix  $\tilde{\mathbf{X}}$  such that the eigenvalue distribution of  $\tilde{\mathbf{X}}$  is

$$\rho_{\tilde{\mathbf{X}}}(\lambda) = \frac{\rho_{\sqrt{\mathbf{X}\mathbf{X}^\top}(\lambda)} + \rho_{\sqrt{\mathbf{X}\mathbf{X}^\top}(-\lambda)}{2} \quad (9)$$

where  $\tilde{\mathbf{X}}$  is symmetrized singular value version of  $\mathbf{X}$ . With the tools of non-Hermitian free probability [2], we present the first main result of the article as follows.

**Result 1.** For all  $z \in \mathbb{C}$  with positive imaginary part, denote  $G_{\mathbf{J}_l \mathbf{J}_l^\top}(z)$  the (limiting) Stieltjes transform of  $\mathbf{J}_l \mathbf{J}_l^\top$  as defined in (8). Then, as  $N \rightarrow \infty$ , we have

$$\sqrt{z} = R_{\tilde{\mathbf{U}}} \left( \sqrt{z} G_{\mathbf{J}_l \mathbf{J}_l^\top}(z) \right) + R_{\widetilde{\mathbf{W}^l \mathbf{D}^l}} \left( \sqrt{z} G_{\mathbf{J}_l \mathbf{J}_l^\top}(z) \right) + \frac{1}{\sqrt{z} G_{\mathbf{J}_l \mathbf{J}_l^\top}(z)}, \quad (10)$$

where  $\tilde{\mathbf{U}}$  is a random Haar unitary matrix and free of  $\mathbf{W}^l \mathbf{D}^l$  (see the detailed deduction in Proof 1 of SM). The correct root is selected by the asymptotic behavior  $G_{\mathbf{J}_l \mathbf{J}_l^\top}(z) \sim \frac{1}{z}$  as  $z \rightarrow \infty$  [20].

##### 3.1.1 Gaussian weights case

Since  $\rho_{\mathbf{D}^l}(z) = (1 - p_l)\delta(z) + p_l\delta(z - 1)$ , we have  $S_{\mathbf{D}^l}(z) = \frac{z+1}{z+p_l}$ , while the S-transform of a scaled Wishart matrix gives  $S_{\mathbf{W}^l (\mathbf{W}^l)^\top} = \frac{1}{\sigma_w^2(z+1)}$ . Using the fact that the trace operator is cyclic-invariant, we deduce

$$S_{\mathbf{W}^l \mathbf{D}^l (\mathbf{W}^l \mathbf{D}^l)^\top}(z) = S_{\mathbf{D}^l \mathbf{W}^l (\mathbf{W}^l)^\top} = S_{\mathbf{D}^l} S_{\mathbf{W}^l (\mathbf{W}^l)^\top} = \frac{1}{\sigma_w^2(z+p_l)}. \quad (11)$$

For a random matrix  $\mathbf{X}$ , the S-transforms of  $\tilde{\mathbf{X}}$  and  $\mathbf{X}\mathbf{X}^\top$  have the following relation [2]:

$$S_{\tilde{\mathbf{X}}}(z) = \sqrt{\frac{z+1}{z} S_{\mathbf{X}\mathbf{X}^\top}(z)}. \quad (12)$$

With (12) we have

$$S_{\tilde{\mathbf{U}}}(z) = \sqrt{\frac{z+1}{z} S_{\mathbf{I}}(z)} = \sqrt{\frac{z+1}{z}}, S_{\widetilde{\mathbf{W}^l \mathbf{D}^l}}(z) = \sqrt{\frac{z+1}{z} S_{\mathbf{W}^l \mathbf{D}^l (\mathbf{W}^l \mathbf{D}^l)^\top}(z)} = \sqrt{\frac{z+1}{\sigma_w^2 z(z+p_l)}}. \quad (13)$$

With the inversion formula between the R-transform and S-transform (7), we have

$$R_{\tilde{\mathbf{U}}}(z) = \frac{1}{2} \left( \sqrt{4 + z^{-2}} - z^{-1} \right), R_{\widetilde{\mathbf{W}^l \mathbf{D}^l}}(z) = \frac{1}{2} \left( -z^{-1} + \sigma_w^2 z + \sqrt{4p_l \sigma_w^2 + (z^{-1} - \sigma_w^2 z)^2} \right). \quad (14)$$

By substituting (14) into (10) and going through some long tedious manipulations, we obtain the following quartic equation for  $G_{\mathbf{J}_l \mathbf{J}_l^\top}$  as

$$c_4 G_{\mathbf{J}_l \mathbf{J}_l^\top}^4 + c_3 G_{\mathbf{J}_l \mathbf{J}_l^\top}^3 + c_2 G_{\mathbf{J}_l \mathbf{J}_l^\top}^2 + c_1 G_{\mathbf{J}_l \mathbf{J}_l^\top} + c_0 = 0 \quad (15)$$

with  $c_4 = \sigma_w^4 z(z-1)$ ,  $c_3 = \sigma_w^2 z((2p_l - 1)\sigma_w^2 - 2z + 2)$ ,  $c_2 = \sigma_w^4 p_l(p_l - 1) + (z-1)^2 - \sigma_w^2(2p_l - 1)(z+1)$ ,  $c_1 = \sigma_w^2$  and  $c_0 = -1$ .

One may further deduce the equation of  $M_{\mathbf{J}_l \mathbf{J}_l^\top}$  by substituting (3) into (15). Although the (explicit) solution is not included here for brevity, the expectation  $\mu_{\mathbf{J}_l \mathbf{J}_l^\top}$  and variance  $\sigma_{\mathbf{J}_l \mathbf{J}_l^\top}^2$  of the limiting eigenvalue density of  $\mathbf{J}_l \mathbf{J}_l^\top$  are concise. Recall the definition of moments  $m_k^{(l)} := \int d\lambda \rho_{\mathbf{J}_l \mathbf{J}_l^\top}(\lambda) \lambda^k$ , with (4) we obtain the closed-form expressions of  $m_1^{(l)}$  and  $m_2^{(l)}$  as

$$m_1^{(l)} = 1 + \sigma_w^2 p_l, \quad m_2^{(l)} = 1 + \sigma_w^2 p_l (4 + \sigma_w^2 + \sigma_w^2 p_l). \quad (16)$$

Since that  $\mu_{\mathbf{J}_l \mathbf{J}_l^\top} = m_1^{(l)}$  and  $\sigma_{\mathbf{J}_l \mathbf{J}_l^\top}^2 = m_2^{(l)} - (m_1^{(l)})^2$ , we have the interesting observation

$$\mu_{\mathbf{J}_l \mathbf{J}_l^\top} = 1 + \sigma_w^2 p_l, \quad \sigma_{\mathbf{J}_l \mathbf{J}_l^\top}^2 = \sigma_w^2 p_l (2 + \sigma_w^2). \quad (17)$$

### 3.1.2 Orthogonal weights case

For orthogonal weights with  $\mathbf{W}^l (\mathbf{W}^l)^\top = \sigma^2 \mathbf{I}$ . From (12) we have,

$$S_{\widetilde{\mathbf{W}^l \mathbf{D}^l}}(z) = \sqrt{\frac{z+1}{z}} S_{\mathbf{W}^l \mathbf{D}^l (\mathbf{W}^l \mathbf{D}^l)^\top}(z) = \sqrt{\frac{z+1}{z}} S_{\mathbf{D}^{l2}}(z) = \sqrt{\frac{(z+1)^2}{\sigma_w^2 z(z+p)}}. \quad (18)$$

With calculations similar to those of (13)-(15), we obtain the following cubic equation for  $G_{\mathbf{J}_l \mathbf{J}_l^\top}$  as

$$c_3 G_{\mathbf{J}_l \mathbf{J}_l^\top}^3 + c_2 G_{\mathbf{J}_l \mathbf{J}_l^\top}^2 + c_1 G_{\mathbf{J}_l \mathbf{J}_l^\top} + c_0 = 0 \quad (19)$$

with  $c_3 = -z(z-1)(\sigma_w^4 + (z-1)^2 - 2\sigma_w^2(z+1))$ ,  $c_2 = z((1-2p_l)\sigma_w^4 - (z-1)^2 + 2\sigma^2(p_l(z+3) - 2))$ ,  $c_1 = -(p_l - 1)p_l\sigma_w^4 - z + z^2 + (p_l - 1)\sigma_w^2(z+1)$  and  $c_0 = z + \sigma_w^2(p_l - 1)$ .

Once again,  $m_1^{(l)}$  and  $m_2^{(l)}$  can be obtained using (4) as

$$m_1^{(l)} = 1 + \sigma_w^2 p_l, \quad m_2^{(l)} = 1 + \sigma_w^2 p_l (4 + \sigma^2 p_l). \quad (20)$$

As a consequence, we conclude, in this orthogonal weights case, that

$$\mu_{\mathbf{J}_l \mathbf{J}_l^\top} = 1 + \sigma_w^2 p_l, \quad \sigma_{\mathbf{J}_l \mathbf{J}_l^\top}^2 = \sigma_w^2 p_l (2 + \sigma_w^2 (1 - p_l)). \quad (21)$$

In Figure 2 and 3 we plot the empirical eigenvalue density of  $\mathbf{J}_l \mathbf{J}_l^\top$  (in purple) and the limiting distribution from (15) and (19) (in red), for Gaussian and orthogonal weights with  $\sigma_w^2 = 0.1$  or 1 and  $p_l = \frac{1}{2}$  or 1.

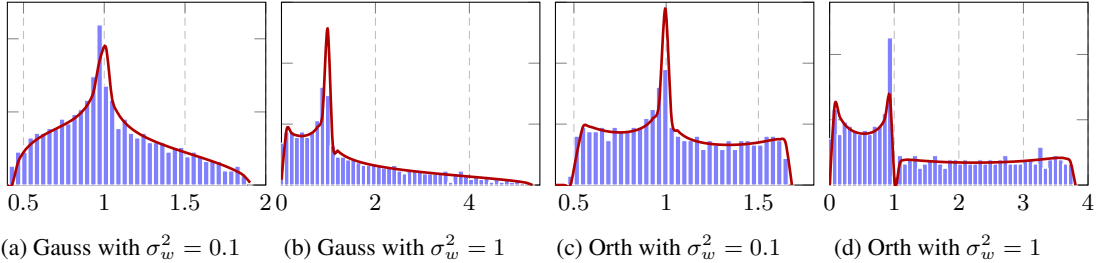


Figure 2: Empirical eigenvalue density (purple) and limiting distribution from (15) and (19) (red) of  $\mathbf{J}_l \mathbf{J}_l^\top$  for Gaussian (a,b) and orthogonal weights (c,d) with  $N = 400$ ,  $p_l = 1/2$ ,  $\sigma_w^2 = 0.1$  and 1.

### 3.2 Extension to the multi-layer case

Following [18, 15], we make a key assumption that the weights in the forward and backward propagation are independent. Since the trace operator is cyclic-invariant, we have

$$S_{\mathbf{J}\mathbf{J}^\top} = S_{\prod_{l=1}^L (\mathbf{I} + \mathbf{W}^l \mathbf{D}^l) (\mathbf{I} + \mathbf{W}^l \mathbf{D}^l)^\top} = S_{\prod_{l=1}^L \mathbf{J}_l \mathbf{J}_l^\top} = \prod_{l=1}^L S_{\mathbf{J}_l \mathbf{J}_l^\top}. \quad (22)$$

We see that the S-transform of  $\mathbf{J}\mathbf{J}^\top$  is simply given by the product of the S-transform of each residual unit  $\mathbf{J}_l \mathbf{J}_l^\top$ . Built upon this observation, the expectation  $\mu_{\mathbf{J}\mathbf{J}^\top}$  and variance  $\sigma_{\mathbf{J}\mathbf{J}^\top}^2$  of the limiting eigenvalue density of  $\mathbf{J}\mathbf{J}^\top$  are given as follows,

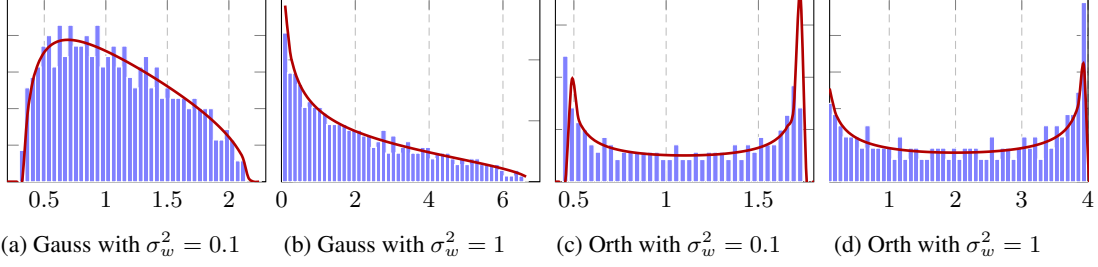


Figure 3: Empirical eigenvalue density (purple) and limiting distribution from (15) and (19) (red) of  $\mathbf{J}_l \mathbf{J}_l^\top$  for Gaussian (a,b) and orthogonal weights (c,d) with  $N = 400$ ,  $p_l = 1$ ,  $\sigma_w^2 = 0.1$  and 1.

**Result 2** (Mean and Variance of the Limiting Spectrum Density). *For  $\mathbf{J} = \prod_{l=1}^L (\mathbf{I}_N + \mathbf{W}^l \mathbf{D}^l)$ , the mean and variance of the limiting eigenvalue density of  $\mathbf{J} \mathbf{J}^\top$  are given by*

$$\mu_{\mathbf{J} \mathbf{J}^\top} = m_1 = \prod_{l=1}^L m_1^{(l)}, \quad \sigma_{\mathbf{J} \mathbf{J}^\top}^2 = m_2 - m_1^2 = \left( \prod_{l=1}^L m_1^{(l)} \right)^2 \sum_{l=1}^L \frac{m_2^{(l)} - (m_1^{(l)})^2}{(m_1^{(l)})^2}, \quad (23)$$

as  $N \rightarrow \infty$ , where we recall  $m^k := \int d\lambda \rho_{\mathbf{J} \mathbf{J}^\top}(\lambda) \lambda^k$ .

We refer the readers to Proof 2 of SM for detailed deduction. To ensure the mean squared singular value of the input-output Jacobian to be of order  $O(1)$  for large  $L$ , we shall have  $\mu_{\mathbf{J} \mathbf{J}^\top} = O(1)$ . This order requirement further indicates that, for both Gaussian and orthogonal weights, we have

$$\sigma_w^2 = O(1/L), \quad (24)$$

by letting  $\prod_{l=1}^L (1 + \sigma_w^2 p_l) = O(1)$ . Since setting  $p_l \rightarrow 0$  implies that almost *all* neurons are inactivated and will lead to a total failure of training, we choose to scale the weights to avoid the problem of exploding or vanishing gradients. With  $\sigma_w^2 = O(1/L)$ , we have  $\sigma_{\mathbf{J} \mathbf{J}^\top}^2 = O(1)$ . Moreover, ensuring that the spectrum of  $\mathbf{J} \mathbf{J}^\top$  is concentrated near 1, i.e.,  $\mu_{\mathbf{J} \mathbf{J}^\top} = 1 + o(1)$  and  $\sigma_{\mathbf{J} \mathbf{J}^\top} = o(1)$ , leads to  $\sigma_w^2 = o(1/L)$ .

In particular, if we consider the linear case (equivalent to have  $p_l = 1$  for all  $l$ ), we obtain the following explicit result on the *full* spectrum of the input-output Jacobian.

**Result 3** (Full Characterization of the Spectrum in Linear Cases). *For Gaussian weights, the Stieltjes transform  $G_{\mathbf{J} \mathbf{J}^\top}$  satisfies,*

$$G_{\mathbf{J} \mathbf{J}^\top} \left( \sqrt{(\sigma_w^2 - 1)^2 + 4\sigma_w^2 z G_{\mathbf{J} \mathbf{J}^\top} + 1 - \sigma_w^2 + 2\sigma_w^2 z G_{\mathbf{J} \mathbf{J}^\top}} \right)^L = 2^L (z G_{\mathbf{J} \mathbf{J}^\top} - 1). \quad (25)$$

*For orthogonal weights, the Stieltjes transform  $G_{\mathbf{J} \mathbf{J}^\top}$  satisfies,*

$$G_{\mathbf{J} \mathbf{J}^\top} \left( (\sigma_w^2 + 1) z G_{\mathbf{J} \mathbf{J}^\top} + \sqrt{(1 - \sigma_w^2)^2 + 4\sigma_w^2 z^2 G_{\mathbf{J} \mathbf{J}^\top}^2} \right)^L = (z G_{\mathbf{J} \mathbf{J}^\top} + 1)^L (z G_{\mathbf{J} \mathbf{J}^\top} - 1). \quad (26)$$

*For both Gaussian and orthogonal weights, taking  $\sigma^2 = c/L$  where  $c$  is a positive constant, we have, as  $L \rightarrow \infty$ ,*

$$\lambda_{\max}(\mathbf{J} \mathbf{J}^\top) = \left( 1 + c + \sqrt{c^2 + 2c} \right) e^{\sqrt{c^2 + 2c}}, \quad (27)$$

*while with  $\sigma = c/L$ , we get instead  $\lambda_{\max}(\mathbf{J} \mathbf{J}^\top) = 1$ .*

We refer the readers to Proof 3 and 4 of SM for detailed calculations.

## 4 Experiments

In this section, we provide empirical evidence to validate the theoretical results in Section 3. Experiments on fully-connected and convolutional ResNets are performed on CIFAR-10 at the early stage of training. Two commonly used optimizers: SGD-Momentum and ADAM [11] are adopted. The observation that two different methods: Momentum and ADAM give very similar results, indicates the robustness of our approach. See Section B in SM for the results of ADAM. Ten repeated experiments are conducted for each setting and the average accuracies are reported here.

## 4.1 Fully-connected ResNet

In this case, the input dimension is reduced to  $N = 400$  with a fully-connected layer of size  $1\,728 \times 400$ . We train a fully-connected ResNet<sup>3</sup> of depth  $L = 100$  and width  $N = 400$  for 1000 steps with a mini-batch size of 128. Three initialization scalings:  $\sigma_w^2 = 1, 1/L$  and  $1/L^2$  are explored here. In Figure 4 we plot the training dynamics for the three initialization scalings of two different nonlinearities with an optimal learning rate of  $10^{-3}$  and a momentum = 0.9.

Based on our theory, an advantage of using layer-dependent scalings of  $\sigma_w^2 = 1/L, 1/L^2$  is claimed over the classical layer-independent scaling  $\sigma_w^2 = 1$ . This claim is confirmed in Figure 4 in which the optimal learning speed is obtained with  $\sigma_w^2 = 1/L^2$  (red) while the worst with  $\sigma_w^2 = 1$  (dark blue). Similar performance is observed in random Gaussian weights in (4a) and orthogonal weights in (4b) with the same nonlinearity and  $\sigma^2$ .

The evolutions of the eigenvalue densities of  $\mathbf{J}\mathbf{J}^T$  are presented in Figure 5. Note that if the well-conditioned spectrum occurs at initialization, this trend tends to continue at the early stage of training. *Dynamical isometry* is achieved with  $\sigma^2 = 1/L^2$ , which leads to the optimal learning speed.

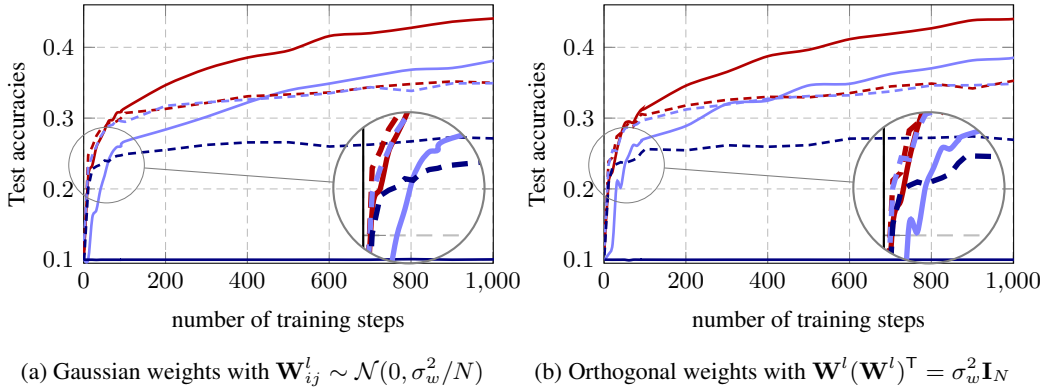


Figure 4: Learning dynamics of a fully-connected ResNet for different initialization scalings  $\sigma_w^2 = 1/L^2$  (red),  $\sigma_w^2 = 1/L$  (purple) and  $\sigma_w^2 = 1$  (dark blue), with a learning rate of  $10^{-3}$ . Solid lines for ReLU and dashed lines for hard-tanh nonlinearity.

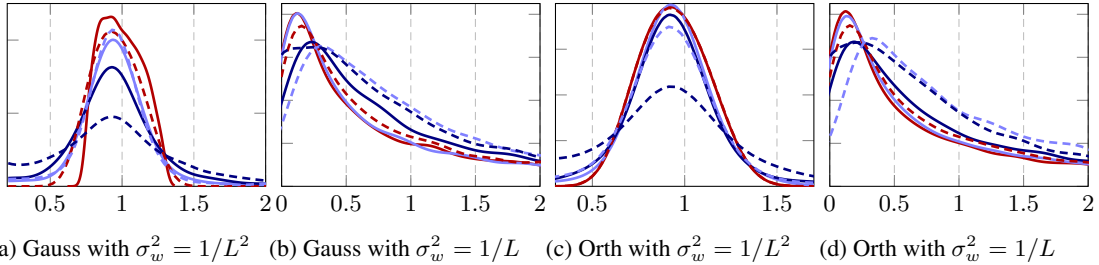


Figure 5: Empirical eigenvalue density of  $\mathbf{J}\mathbf{J}^T$  for Gaussian and orthogonal weights with ReLU in solid and hard-tanh in dashed. For  $\sigma_w^2 = 1/L^2$  in (a)(c) and  $\sigma_w^2 = 1/L$  in (b)(d), each at three different training steps of 1 (red), 100 (purple) and 1000 (dark blue).

## 4.2 Convolutional ResNet

We conduct the experiment based on the ResNet-110 structure as in [9]. In this convolutional ResNet, each residual unit contains a shallow network of 2 layers, and therefore three scalings of  $\sigma_w^2 = 1, 1/\sqrt{L}$  and  $1/L$  are tested (by considering the Jacobian of *all* residual units). For these three choices of  $\sigma_w^2$ , the best performance is always achieved by the learning rate of  $10^{-2}$  with momentum = 0.9 and is presented in Figure 6. We refer the reader to Section B.2 in SM for the results of the

<sup>3</sup> In fully-connected case, every residual unit contains a single layer without batch normalization.

ADAM optimizer. We observe from Figure 6 that: 1) for convolutional ResNet without BN, the magnitude of  $\sigma^2$  plays a central role in obtaining a satisfying learning speed. The optimal learning speed is achieved with  $\sigma^2 = 1/\sqrt{L}$ , while large  $\sigma^2 = 1$  without BN results in exploding gradient and hence the failure of training. Surprisingly, small  $\sigma^2 = 1/\sqrt{L}$  without the regularization effect of the BN [10] *still* has roughly the same performance as  $\sigma^2 = 1$  with BN. 2) it is noteworthy that, different from the fully-connected case, for the convolutional ResNet of 2 layers in each residual unit, the scaling  $\sigma^2 = 1/\sqrt{L}$  always outperforms  $\sigma^2 = 1/L$  while the latter achieves the *dynamical isometry*. This observation is not trivial and comes possibly from the fact that extremely small  $\sigma_w^2$  causes the internal gradient vanishing inside each residual unit. We will discuss this point in the next section.

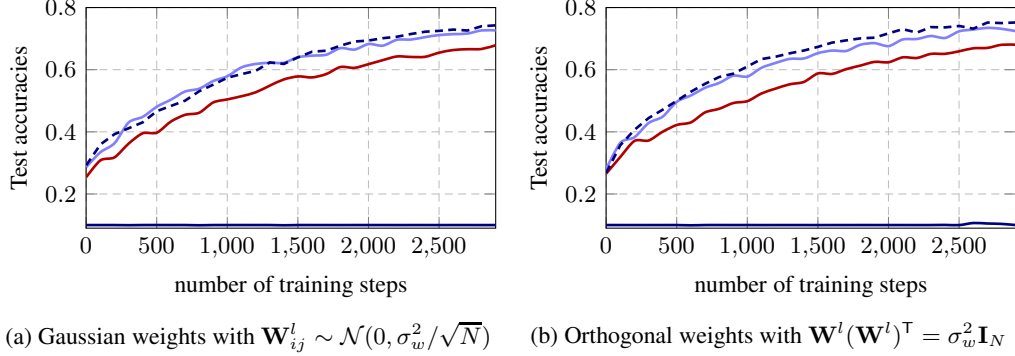


Figure 6: Learning dynamics of a convolutional ResNet for different initialization scalings  $\sigma_w^2 = 1/L$  (red),  $\sigma_w^2 = 1/\sqrt{L}$  (purple) and  $\sigma_w^2 = 1$  (dark blue), with a learning rate of  $10^{-2}$  and the ReLU nonlinearity. Solid lines without BN and dashed ones with the BN procedure added (for  $\sigma_w^2 = 1$ ).

## 5 Discussion and Conclusion

In this article, exploiting advanced tools in free probability in the regime of a large network, we prove that, for ResNets, the variance of the initial random weights should *also* be scaled as a function of the number of layers. More concretely, the theoretical results show that for large  $L$  the condition for spectrum concentration is in fact *universal* in the sense that, for both types of non-linearity (ReLU or hard-tanh) and both weight initialization methods (Gaussian or orthogonal), it suffices to take  $\sigma_w^2 = O(L^{-1})$  to ensure the mean squared singular value of the input-output Jacobian to be of order  $O(1)$  (thus is neither vanishing nor exploding). The weights scaling essentially results in the *eigenspectrum concentration* of  $\mathbf{J}\mathbf{J}^\top$ , such that the error vector will be properly preserved under backpropagation. We then provide in Section 4 the comparison of empirical evidences with our theoretical results. Mathematically speaking, our approach holds only asymptotically as  $N, L \rightarrow \infty$ , practical advantages are observed for finite width  $N$  and depth  $L$ , when applied to the popular CIFAR-10 dataset, for both fully-connected and convolutional ResNets. This agreement is not surprising, as observed in many other fields [19, 20].

In practice, a residual unit always contains a shallow network with  $m$  layers. In this way, the dynamic of the ResNet is given by

$$\begin{cases} \mathbf{h}_1^l &= \mathbf{W}_1^l \phi(\mathbf{x}^{l-1}) + \mathbf{b}_1^l, \dots, \mathbf{h}_m^l = \mathbf{W}_m^l \phi(\mathbf{h}_{m-1}^l) + \mathbf{b}_m^l, \\ \mathbf{x}^l &= \mathbf{x}^{l-1} + \mathbf{h}_m^l. \end{cases} \quad (28)$$

The entire input-output Jacobian matrix is  $\mathbf{J} = \prod_{l=1}^L (\mathbf{I}_N + \hat{\mathbf{J}}_l)$ , where  $\hat{\mathbf{J}}_l = \frac{\partial \mathbf{h}_m^l}{\partial \mathbf{x}^{l-1}} = \prod_{i=1}^m \mathbf{W}_i^l \mathbf{D}_i^l$  denotes the local Jacobian matrix of a residual unit. For  $m > 1$ , let  $\sigma^2 = O(L^{-1/m})$  and the spectrum of  $\mathbf{J}\mathbf{J}^\top$  will be well-conditioned. However, the eigenvalues of the local Jacobian matrix  $\hat{\mathbf{J}}_l \hat{\mathbf{J}}_l^\top$  will be extremely small and cause the gradient vanishing in the local residual unit. Thus, a *trade-off* between the entire and local input-output Jacobian matrix is always required.



In future work, it would be interesting to extend our theoretical framework to more general skip connections. Moreover, exploring new weight initializations or nonlinearities to handle the *trade-off* mentioned above would be of practical significance.

## References

- [1] G Akemann, J. R. Ipsen, and M Kieburg. Products of rectangular random matrices: singular values and progressive scattering. Phys Rev E Stat Nonlin Soft Matter Phys, 88(5):052118, 2013.
- [2] Burak Cakmak. Non-hermitian random matrix theory for mimo channels. Institutt for Elektronikk Og Telekommunikasjon, 2012.
- [3] Ronan Collobert and Jason Weston. A unified architecture for natural language processing: Deep neural networks with multitask learning. In Proceedings of the 25th international conference on Machine learning, pages 160–167. ACM, 2008.
- [4] Giovanni Ferraro. Lagrange inversion theorem. Springer New York, 2008.
- [5] Xavier Glorot and Yoshua Bengio. Understanding the difficulty of training deep feedforward neural networks. In Proceedings of the thirteenth international conference on artificial intelligence and statistics, pages 249–256, 2010.
- [6] Moritz Hardt and Tengyu Ma. Identity matters in deep learning. 2016.
- [7] Kaiming He, Xiangyu Zhang, Shaoqing Ren, and Jian Sun. Delving deep into rectifiers: Surpassing human-level performance on imagenet classification. pages 1026–1034, 2015.
- [8] Kaiming He, Xiangyu Zhang, Shaoqing Ren, and Jian Sun. Deep residual learning for image recognition. In Computer Vision and Pattern Recognition, pages 770–778, 2016.
- [9] Kaiming He, Xiangyu Zhang, Shaoqing Ren, and Jian Sun. Identity mappings in deep residual networks. pages 630–645, 2016.
- [10] Sergey Ioffe and Christian Szegedy. Batch normalization: Accelerating deep network training by reducing internal covariate shift. arXiv preprint arXiv:1502.03167, 2015.
- [11] Diederik P Kingma and Jimmy Ba. Adam: A method for stochastic optimization. Computer Science, 2014.
- [12] Alex Krizhevsky, Ilya Sutskever, and Geoffrey E Hinton. Imagenet classification with deep convolutional neural networks. In Advances in neural information processing systems, pages 1097–1105, 2012.
- [13] Abdel-rahman Mohamed, George E Dahl, and Geoffrey Hinton. Acoustic modeling using deep belief networks. IEEE Transactions on Audio, Speech, and Language Processing, 20(1):14–22, 2012.
- [14] Alexandru Nica and Roland Speicher. Lectures on the combinatorics of free probability. Cambridge Uk, 2006.
- [15] Jeffrey Pennington, Samuel S. Schoenholz, and Surya Ganguli. Resurrecting the sigmoid in deep learning through dynamical isometry: theory and practice. 2017.
- [16] Jeffrey Pennington, Samuel S. Schoenholz, and Surya Ganguli. The emergence of spectral universality in deep networks. 2018.
- [17] Andrew M Saxe, James L McClelland, and Surya Ganguli. Exact solutions to the nonlinear dynamics of learning in deep linear neural networks. Computer Science, 2013.
- [18] Samuel S. Schoenholz, Justin Gilmer, Surya Ganguli, and Jascha Sohl-dickstein. Deep information propagation. 2017.
- [19] J. W. Silverstein. Spectral analysis of large dimensional random matrices. Science Press,, 2010.
- [20] Terence Tao. Topics in Random Matrix Theory. American Mathematical Society,, 2012.

## A Theoretical Results

**Proof 1** (The deduction of (10)). The following equation establishes the bridge between  $\widetilde{\mathbf{X}}$  and  $\mathbf{X}\mathbf{X}^\top$ ,

$$G_{\widetilde{\mathbf{X}}}(z) = zG_{\mathbf{X}\mathbf{X}^\top}(z^2), \quad (29)$$

A random matrix  $\mathbf{X}$  is called R-diagonal if it can be decomposed as  $\mathbf{X} = \mathbf{U}\mathbf{Y}$ , such that  $\mathbf{U}$  is Haar unitary and free of  $\mathbf{Y} = \sqrt{\mathbf{X}\mathbf{X}^\top}$ . If the free random matrices  $\mathbf{X}$  and  $\mathbf{Y}$  be R-diagonal, then we have,

$$R_{\widetilde{\mathbf{X}+\mathbf{Y}}} = R_{\widetilde{\mathbf{X}}} + R_{\widetilde{\mathbf{Y}}}. \quad (30)$$

According to [2], we have

$$G_{\mathbf{J}_l\mathbf{J}_l^\top} = G_{(\mathbf{I}+\mathbf{W}^l\mathbf{D}^l)(\mathbf{I}+\mathbf{W}^l\mathbf{D}^l)^\top} = G_{(\mathbf{U}+\mathbf{W}^l\mathbf{D}^l)(\mathbf{U}+\mathbf{W}^l\mathbf{D}^l)^\top}, \quad (31)$$

where  $\mathbf{U}$  is a random Haar unitary matrix and free of  $\mathbf{W}^l\mathbf{D}^l$ .

Note that  $\widetilde{\mathbf{U}}$  and  $\widetilde{\mathbf{W}^l\mathbf{D}^l}$  are R-diagonal, with (30) we have,

$$R_{\widetilde{\mathbf{U}+\mathbf{W}^l\mathbf{D}^l}}(z) = R_{\widetilde{\mathbf{U}}}(z) + R_{\widetilde{\mathbf{W}^l\mathbf{D}^l}}(z). \quad (32)$$

According to the definition of R-transform, we have,

$$z = R_{\widetilde{\mathbf{U}}}\left[G_{\widetilde{\mathbf{U}+\mathbf{W}^l\mathbf{D}^l}}(z)\right] + R_{\widetilde{\mathbf{W}^l\mathbf{D}^l}}\left[G_{\widetilde{\mathbf{U}+\mathbf{W}^l\mathbf{D}^l}}(z)\right] + \frac{1}{G_{\widetilde{\mathbf{U}+\mathbf{W}^l\mathbf{D}^l}}(z)} \quad (33)$$

With (29), we have,

$$G_{\mathbf{J}_l\mathbf{J}_l^\top} = G_{(\mathbf{U}+\mathbf{W}^l\mathbf{D}^l)(\mathbf{U}+\mathbf{W}^l\mathbf{D}^l)^\top}(z) = \frac{1}{\sqrt{z}}G_{\widetilde{\mathbf{U}+\mathbf{W}^l\mathbf{D}^l}}(\sqrt{z}). \quad (34)$$

With (33) and (34), we have the following equation that the Stieljes transform  $G_{\mathbf{J}_l\mathbf{J}_l^\top}(z)$  satisfies,

$$\sqrt{z} = R_{\widetilde{\mathbf{U}}}\left[\sqrt{z}G_{\mathbf{J}_l\mathbf{J}_l^\top}(z)\right] + R_{\widetilde{\mathbf{W}^l\mathbf{D}^l}}\left[\sqrt{z}G_{\mathbf{J}_l\mathbf{J}_l^\top}(z)\right] + \frac{1}{\sqrt{z}G_{\mathbf{J}_l\mathbf{J}_l^\top}(z)}. \quad (35)$$

**Proof 2** (Multi-layer case). Since

$$M_{\mathbf{J}_l\mathbf{J}_l^\top} = \frac{m_1^{(l)}}{z} + \frac{m_2^{(l)}}{z^2} + \dots. \quad (36)$$

Employ the Lagrange inversion theorem and we have,

$$M_{\mathbf{J}_l\mathbf{J}_l^\top}^{-1} = \frac{m_1^{(l)}}{z} + \frac{m_2^{(l)}}{m_1^{(l)}} + \dots. \quad (37)$$

Thus,

$$S_{\mathbf{J}_l\mathbf{J}_l^\top} = \frac{1+z}{zM_{\mathbf{J}_l\mathbf{J}_l^\top}^{-1}} = \frac{1}{m_1^{(l)}} + \left(\frac{1}{m_1^{(l)}} - \frac{m_2^{(l)}}{(m_1^{(l)})^3}\right)z + \dots, \quad (38)$$

Thus,

$$S_{\mathbf{J}\mathbf{J}^\top} = \prod_{l=1}^L S_{\mathbf{J}_l\mathbf{J}_l^\top} = \prod_{l=1}^L \frac{1}{m_1^{(l)}} + \sum_{j=1}^L \left[ \left( \frac{(m_1^{(j)})^2 - m_2^{(j)}}{(m_1^{(j)})^2} \right) \prod_{l=1}^L \frac{1}{m_1^{(l)}} \right] z + \dots. \quad (39)$$

For the sake of simplicity, let  $X \equiv \prod_{l=1}^L \frac{1}{m_1^{(l)}}$  and  $Y \equiv \sum_{j=1}^L \left[ \left( \frac{(m_1^{(j)})^2 - m_2^{(j)}}{(m_1^{(j)})^2} \right) \prod_{l=1}^L \frac{1}{m_1^{(l)}} \right]$ .

Expand  $M_{\mathbf{J}\mathbf{J}^\top}^{-1}$  and we have,

$$M_{\mathbf{J}\mathbf{J}^\top}^{-1} = \frac{1+z}{zS_{\mathbf{J}\mathbf{J}^\top}} = \frac{1}{Xz} + \frac{X-Y}{X^2} + \dots. \quad (40)$$

Let  $m^k := \int d\lambda \rho_{\mathbf{J}\mathbf{J}^\top}(\lambda) \lambda^k$ , we obtain the following equations:

$$m_1 = \frac{1}{X} = \prod_{l=1}^L m_1^{(l)}, \quad m_2 = \frac{X - Y}{X^3}. \quad (41)$$

Finally, we obtain the expectation  $\mu_{\mathbf{J}\mathbf{J}^\top}$  and variance  $\sigma_{\mathbf{J}\mathbf{J}^\top}^2$  of  $\mathbf{J}\mathbf{J}^\top$ ,

$$\begin{aligned} \mu_{\mathbf{J}\mathbf{J}^\top} &= m_1 = \prod_{l=1}^L m_1^{(l)}, \\ \sigma_{\mathbf{J}\mathbf{J}^\top}^2 &= m_2 - m_1^2 = \left( \prod_{l=1}^L m_1^{(l)} \right)^2 \sum_{l=1}^L \frac{m_2^{(l)} - \left(m_1^{(l)}\right)^2}{\left(m_1^{(l)}\right)^2}. \end{aligned} \quad (42)$$

**Proof 3** (Full Characterization of the Spectrum in Linear Cases: Gaussian Case). As  $p_1 = \dots = p_L = 1$ , the quadric equation (15) is simplified as,

$$\sigma_w^4 z G_{\mathbf{J}_i \mathbf{J}_i^\top}^3(z) - 2\sigma_w^2 z G_{\mathbf{J}_i \mathbf{J}_i^\top}^2(z) + (\sigma_w^2 + z - 1) G_{\mathbf{J}_i \mathbf{J}_i^\top}(z) - 1 = 0, \quad (43)$$

which leads to

$$S_{\mathbf{J}_i \mathbf{J}_i^\top} = \frac{2}{\sqrt{(\sigma_w^2 + 1)^2 + 4\sigma_w^2 z + 1 + \sigma_w^2 + 2\sigma_w^2 z}}. \quad (44)$$

Thus,

$$S_{\mathbf{J}\mathbf{J}^\top} = \left( S_{\mathbf{J}_i \mathbf{J}_i^\top} \right)^L = \left( \frac{2}{\sqrt{(\sigma_w^2 + 1)^2 + 4\sigma_w^2 z + 1 + \sigma_w^2 + 2\sigma_w^2 z}} \right)^L. \quad (45)$$

The S-transform and the Stieltjes transform of a random matrix  $\mathbf{X}$  has the following equation,

$$S_{\mathbf{X}}(z G_{\mathbf{X}} - 1) = \frac{G_{\mathbf{X}}}{z G_{\mathbf{X}} - 1}. \quad (46)$$

Thus, we have the equation of  $G_{\mathbf{J}\mathbf{J}^\top}$  as follows,

$$G_{\mathbf{J}\mathbf{J}^\top} \left( \sqrt{(\sigma_w^2 - 1)^2 + 4\sigma_w^2 z G_{\mathbf{J}\mathbf{J}^\top}} + 1 - \sigma_w^2 + 2\sigma_w^2 z G_{\mathbf{J}\mathbf{J}^\top} \right)^L = 2^L (z G_{\mathbf{J}\mathbf{J}^\top} - 1). \quad (47)$$

To obtain the max eigenvalue, we use a trick [1] by multiplying  $z$  on the both size of (47),

$$z G_{\mathbf{J}\mathbf{J}^\top} \left( \sqrt{(\sigma_w^2 - 1)^2 + 4\sigma_w^2 z G_{\mathbf{J}\mathbf{J}^\top}} + 1 - \sigma_w^2 + 2\sigma_w^2 z G_{\mathbf{J}\mathbf{J}^\top} \right)^L = 2^L z (z G_{\mathbf{J}\mathbf{J}^\top} - 1). \quad (48)$$

For simplicity, let  $u = z G_{\mathbf{J}\mathbf{J}^\top}$  and  $Y = \sqrt{(\sigma_w^2 - 1)^2 + 4\sigma_w^2 u} + 1 - \sigma_w^2 + 2\sigma_w^2 u$ . Then (48) can be rewritten as,

$$\frac{u Y^L}{u - 1} = 2^L z. \quad (49)$$

Note that  $\frac{dz}{dG} = 0$  at the endpoints of support of the spectrum [1]. By differentiating both sides of (49), we have

$$Y^L + Lu Y^{L-1} \left( \frac{2\sigma_w^2}{\sqrt{(\sigma_w^2 - 1)^2 + 4su}} + 2\sigma_w^2 \right) = 2^L z. \quad (50)$$

The equation of  $u$  can be obtained with (49) and (50),

$$Lu \left( \frac{2\sigma_w^2}{\sqrt{(\sigma_w^2 - 1)^2 + 4\sigma_w^2 u}} + 2\sigma_w^2 \right) = \frac{\sqrt{(\sigma_w^2 - 1)^2 + 4\sigma_w^2 u} + 1 - \sigma_w^2 + 2\sigma_w^2 u}{u - 1}. \quad (51)$$

Solve (51) and substitute  $u$  to (49) will lead to the final result.

**Proof 4** (Full Characterization of the Spectrum in Linear Cases: Orthogonal Case). As  $p_1 = \dots = p_L = 1$ , the cubic equation (19) is simplified as,

$$G_{\mathbf{J}_i \mathbf{J}_i^\top}(z) = \frac{1}{z-1} \sqrt{\frac{(z-1)^2}{\sigma_w^4 - 2\sigma_w^2(z+1) + (z-1)^2}}. \quad (52)$$

Then, the S-transform of  $\mathbf{J}_i \mathbf{J}_i^\top$  is

$$S_{\mathbf{J}_i \mathbf{J}_i^\top}(z) = \frac{z+2}{(\sigma_w^2+1)(z+1) + \sqrt{(1+\sigma_w^2)^2 + 4\sigma_w^2 z(z+2)}}. \quad (53)$$

With (46), we have the equation of  $G_{\mathbf{J} \mathbf{J}^\top}$  as follows,

$$(zG_{\mathbf{J} \mathbf{J}^\top} - 1) \left( \frac{zG_{\mathbf{J} \mathbf{J}^\top} + 1}{(\sigma_w^2 + 1)zG_{\mathbf{J} \mathbf{J}^\top} + \sqrt{(1 - \sigma_w^2)^2 + 4\sigma_w^2 z^2 G_{\mathbf{J} \mathbf{J}^\top}^2}} \right)^L = G_{\mathbf{J} \mathbf{J}^\top}. \quad (54)$$

Letting  $u = zG_{\mathbf{J} \mathbf{J}^\top}$ ,  $Y = \sqrt{(1 - \sigma_w^2)^2 + 4\sigma_w^2 u^2}$  and using the same trick as above, we have

$$u \left( \frac{(\sigma_w^2 + 1)u + Y}{u + 1} \right)^L = z(u - 1), \quad (55)$$

$$Lu \left( 1 + \sigma_w^2 + \frac{4\sigma_w^2 u}{Y} - \frac{(1 + \sigma_w^2)u + Y}{1 + u} \right) = \frac{(1 + \sigma_w^2)u + Y}{u - 1}. \quad (56)$$

Solve (56) and substitute  $u$  to (55) will lead to the final result.

## B Complementary Experiments Results with ADAM Optimizer

### B.1 Fully-connected ResNets

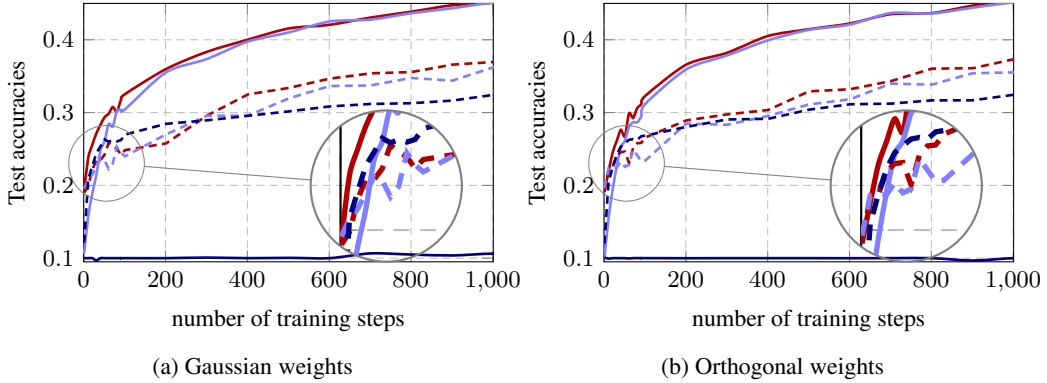


Figure 7: Learning dynamics of a fully-connected ResNet for different initialization scalings  $\sigma_w^2 = 1/L^2$  (red),  $\sigma_w^2 = 1/L$  (purple) and  $\sigma_w^2 = 1$  (blue), with a learning rate of  $10^{-4}$ . Solid lines for ReLU and dashed lines for hard-tanh nonlinearity.

### B.2 Convolutional ResNet

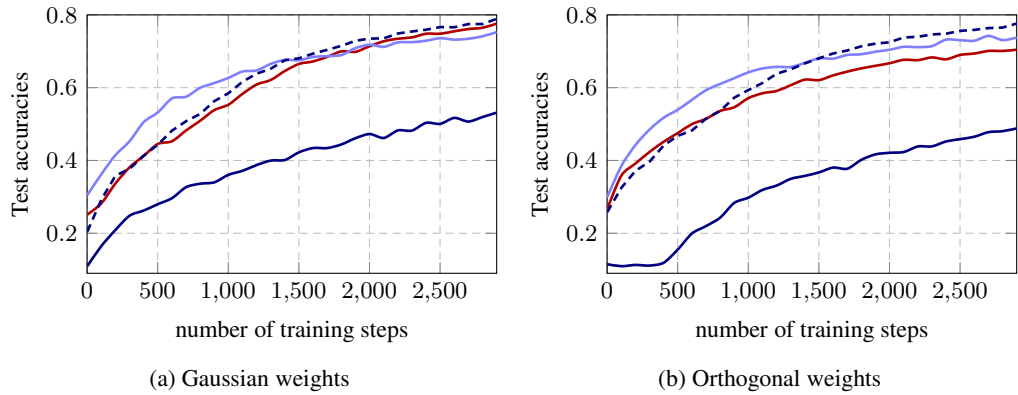


Figure 8: Learning dynamics of a convolutional ResNet for different initialization scalings  $\sigma_w^2 = 1/L$  (red),  $\sigma_w^2 = 1/\sqrt{L}$  (purple) and  $\sigma_w^2 = 1$  (blue), with a learning rate of  $10^{-2}$  and the ReLU nonlinearity. Solid lines without BN and dashed ones with the BN procedure added (for  $\sigma_w^2 = 1$ ).